

Vision in observers with enhanced S-cone syndrome: an excess of S-cones but connected mainly to conventional S-cone pathways

Caterina Ripamonti, Jonathan Aboshiha, G. Bruce Henning, Panagiotis I. Sergouniotis, Michel Michaelides, Anthony T. Moore, Andrew R. Webster, and Andrew Stockman

UCL Institute of Ophthalmology, University College London, 11-43 Bath Street, London EC1V 9EL, England

ABSTRACT

Purpose:

The effect of increased numbers of S-cone photoreceptors in enhanced S-cone syndrome (ESCS) was investigated psychophysically in six ESCS observers to understand more about the relative cone sensitivities and postreceptoral organization.

Methods:

Measures of temporal sensitivity or delay were made: S- and L-cone temporal acuity (critical flicker fusion or cff), S-cone temporal contrast sensitivity, and S-cone delay.

Results:

ESCS observers showed uniform enhancements of S-cone cff of between 0.85 and 6.25 Hz, but reductions in L-cone cff. They also showed higher S-cone temporal-contrast-sensitivities at medium and high S-cone adaptation levels with sensitivity functions that peaked near 7.5 Hz but fell off at lower and higher frequencies; in contrast, the mean normal function was flat at low frequencies and fell-off only at high frequencies. The S-cone signal, as in the normal, is subject to large phase delays.

Conclusions:

We interpret the enhancements in cff as increases in S-cone number in ESCS of between 1.39 and 11.32 times normal density (with a mean of 3.48). The peaked ESCS contrast-sensitivity functions are consistent with S-cone signal interactions that increase sensitivity at intermediate frequencies through constructive interference but decrease it at lower and higher frequencies through destructive interference. Measurements of S-cone delays relative to L- and M-cone signals show that the predominant S-cone signals in ESCS are negative and delayed as in normal observers, but reveal another faster, positive S-cone signal. This signal is also likely to be the cause of constructive and destructive interference in the contrast-sensitivity data of ESCS observers.

Keywords: Enhanced S-cone syndrome, flicker sensitivity, critical flicker fusion, temporal processing, *NR2E3*, temporal acuity, short-wavelength-sensitive cones.

INTRODUCTION

Enhanced S-cone syndrome (ESCS) is a rare inherited degenerative retinal disease named after the associated unusual gain in function—an increase in short-wavelength-sensitive (S-) cone sensitivity.¹ The syndrome is also characterised by severely reduced rod sensitivity (night blindness), foveal schisis and macular cysts, varying degree of visual acuity loss, and atypical electroretinograms (ERGs) that show little or no responses to dim rod (scotopic) stimuli, but have large, slow responses to brighter cone (photopic) stimuli.¹⁻⁴ The photopic ERG was originally thought to be of rod origin,⁵⁻⁷ but spectral measurements have shown that it is dominated by S-cones with reduced contributions from long- and middle-wavelength-sensitive (L- and M-) cones.^{2, 8, 9} Psychophysical studies also show increased short-wavelength and decreased middle- and long-wavelength sensitivities consistent with S-cone enhancement and L- and M-cone impairment; moreover, the increased sensitivities on yellow adapting fields have an S-cone spectral sensitivity.^{2, 3, 10} Despite the reduction in L- and M-cone sensitivity, colour vision in ESCS observers assessed by standard tests is usually normal;^{1, 3} but some deficits have been reported.¹¹

The increased S-cone sensitivity has been linked to a larger than normal number of S-cones in the retinae of ESCS patients.^{9, 10, 12} Hood *et al.*⁹ estimated that S-cone ERG a-waves in ESCS affected individuals, which are 4-6 times bigger than normal, are consistent with as many as 75 times more S-cones than normal in the affected retinae. A modest improvement in S-cone acuity has also been reported, but only with high adaptation levels of “yellow” background light where the normal S-cone acuity falls but that of ESCS observers does not.¹⁰ More direct evidence for a relative increase in the number of S-cones was provided by histological examination of a disordered ESCS retina of a 77-year old woman,¹² in which twice the normal number of cones was found, 92% of which were S-cones. A more recent study used adaptive optics imaging to attempt to visualise individual cones directly *in vivo* in three young adults with ESCS.¹³ The authors found a disordered cone mosaic, but were unable to quantify either cone-cell density or type.

The excess of S-cones can be related to a molecular defect. The gene *NR2E3* codes for a photoreceptor-specific nuclear receptor NR2E3^{12, 14, 15} that, acting in concert with CRX and NRL, is thought to promote the differentiation and survival of rod photoreceptors by regulating the transcription of rod- and cone-specific genes, and, in particular, repressing the expression of cone-

specific genes in rods that would otherwise favour an S-cone fate for the precursor cell.^{12, 16-19} More than thirty different mutations of *NR2E3* have been linked to ESCS, Goldmann-Favre syndrome, and clumped pigmentary retinal degeneration.²⁰⁻²³

One goal of this work is to characterize the disorder more fully by measuring temporal acuity for S-cone and L-cone-detected flicker in ESCS affected individuals and by measuring S-cone temporal contrast sensitivity functions. These S-cone measurements may reveal the postreceptoral organization of S-cone signals in ESCS observers, and, in particular, whether the postreceptoral organization differs from normal.

In normal observers, under conditions where L- and M-cone-detected flicker can be resolved up to 50 Hz,^{24, 25} S-cone-detected flicker can be perceptually resolved up to only 18 to 28 Hz,²⁶⁻²⁸ (Under the conditions of our experiment, L-cone flicker can be resolved in normal observers up to a frequency of about 40 Hz; see Figure 2, below.) These sensitivities depend on both receptor and postreceptoral properties of the S-cone, and on the L- and M-cone pathways. Given that the S-cone photoreceptors are as fast as their L- and M-cone counterparts,^{9, 29-31} the perceptual differences between the S- and L/M-cone sensitivities in normal observers must be due to postreceptoral differences.^{32, 33} And, indeed, under most conditions in normal observers, the S-cone signals seem to be confined to sluggish visual pathways with low-pass temporal-frequency responses that carry chromatic information with little or no access to the faster pathways that carry luminance or intensity information.³⁴⁻⁴³ However, under some conditions of long-wavelength adaptation often used to isolate the S-cone response (such as those used here), S-cone signals make a delayed, *negative* contribution to fast luminance pathways, probably by way of some indirect connection, perhaps via horizontal cells.^{28, 44-46}

Given the excess of S-cones in the ESCS retinae, it is conceivable that some S-cones may displace the direct L- and M-cone inputs into the luminance pathway. And, because the normal luminance pathway consists of fast, positive contributions from the L- and M- pathways, we should then expect to find evidence in individuals with ESCS for a much greater S-cone temporal signal that also makes a *positive* contribution to luminance. If, instead, the normal postreceptoral organization is preserved, the S-cone contribution in the ESCS observer should be delayed and negative just as it is in normal observers. Further, S-cone temporal sensitivity measures in ESCS observers might be expected to show modest improvements that are consistent with an increase in the numbers of S-cones, rather than large improvements indicative of a change to a faster pathway.

Our results suggest that while the predominant S-cone pathway in ESCS corresponds to the same pathway found in normals, evidence for a second, faster pathway can be found in the temporal contrast-sensitivity and phase-delay data.

GENERAL METHODS

Observers

The experimental group of observers comprised six individuals with ESCS. All had a history of night blindness, maculopathy, and relatively mild peripheral visual field loss. The availability of ESCS-observers constrained how many of the experiments each could perform: All six ESCS observers participated in the S-cone cff measurements, ES1-ES4 participated in the L-cone cff measurements, and only ES1-ES3 participated in the S-cone temporal contrast-sensitivity and phase-delay measurements. The stimuli were presented to the observers' right eye, except for observers ES1 and ES6, who preferred to use their left eyes. A group of up to 12 adults with normal or corrected to normal visual acuity provided representative control data. All participants, including the ESCS individuals, had normal colour vision as assessed by the Farnsworth-Munsell 100-hue test, and by red-green Rayleigh and blue-green Moreland anomaloscope matches.

This study conformed to the standards set by the Declaration of Helsinki, and the procedures have been approved by local ethics committees at Moorfields Eye Hospital and at University College London.

The sequence-variants identified in *NR2E3* in the six ESCS observers, their age at the time of testing, and their right and left eye acuities are as follows:

ES1	IVS1-2A>C, p.E341K	37	6/24 OD, 6/36 OS
ES2	p.R311Q, p.L371W	29	6/9 OD, 6/9 OS
ES3	IVS1-2A>C, p.A256E	39	6/9 OD, 6/9 OS
ES4	Unknown	32	6/12 OD, 6/18 OS
ES5	IVS1-2A>C homozygous	28	6/9 OD, 6/12 OS
ES6	IVS1-3A>G homozygous	27	3/60 OD, 6/60 OS

Apparatus

We used a conventional Maxwellian-view optical system with a 2-mm entrance pupil illuminated by a 900-W Xenon arc lamp. Wavelengths were selected by the use of interference filters with full-width at half-maximum bandwidths of between 7 and 11 nm (Ealing or Oriel). The radiance of each beam could be controlled by the insertion of fixed neutral density filters (Oriel) or by the rotation of circular, variable neutral-density filters (Rolyn Optics). Sinusoidal modulation was generated by pulse-width modulation of fast, liquid-crystal, light shutters running at 400 Hz with rise and fall times faster than 50 μ s (Displaytech), thus effectively producing rectangular pulses of variable width at a fixed frequency of 400 Hz. The pulse-width was varied sinusoidally under computer control using programmable timers (Data Translation, DT2819) to produce the sinusoidal stimuli at the desired *visible* frequencies and at signal modulations up to 92%. (Frequencies near the 400-Hz rectangular-pulse frequency and above were much too high to be resolved, so that observers saw only the sinusoidally-varying stimuli produced by the variation of the pulse-width.)

The position of the observer's head was maintained by a dental wax impression fixed to a milling-machine head that could be moved in three dimensions to align the observer's pupil in the optical system. The system is described in full detail elsewhere.⁴⁷

Stimuli

Visual targets were centrally-fixated, monochromatic, 4° diameter discs that flickered sinusoidally about a fixed mean radiance, \bar{R} . The flickering waveform was thus given by:

$$A(t) = \bar{R}[1 + m \sin(2\pi ft + \theta)], \quad [1]$$

where f is the frequency of the flicker (in Hz), θ is the phase, and, the ripple ratio or “modulation”, m , is defined as the conventional Michelson contrast:

$$m = \frac{I_{max} - I_{min}}{I_{max} + I_{min}}. \quad [2]$$

I_{max} and I_{min} are the maximum and minimum radiances of the stimulus, respectively. The maximum target modulation that could be achieved was 92%. Fixation was always central.

S-cone measurements. A flickering 4° diameter target of 440 nm was presented in the centre of a steady, 9° diameter, 620-nm background field. The radiance of the background was fixed at 11.41 \log_{10} quanta $s^{-1} \text{ deg}^{-2}$. This background selectively desensitizes the M- and L-cones, but has comparatively little direct effect on the S-cones. For normal observers, the background ensures that flicker detection is mediated by the S-cones up to a target radiance of about 10.0 \log_{10} quanta s^{-1}

deg^{-2} ^{28, 31, 48}. Above $10.0 \log_{10} \text{ quanta s}^{-1} \text{ deg}^{-2}$, M-cones may also contribute to flicker detection in normal observers. In the ESCS observers, who have reduced L- and M-cone sensitivities (see Figure 2), any M-cone contribution will occur at still higher radiances or not at all.

Three types of S-cone measurement were made, each described in more details below: critical flicker fusion (cff), temporal contrast-sensitivity measurements, and phase delay measurements.

L-cone measurements. A flickering 4° diameter target of 650-nm wavelength was presented in the centre of a 9° , 481-nm background field. The radiance of the 481-nm background was $8.26 \log \text{ quanta s}^{-1} \text{ deg}^{-2}$ ($1.39 \log_{10}$ photopic trolands or $2.53 \log_{10}$ scotopic trolands). The 650-nm target wavelength was chosen to favour detection by L-cones rather than rods or S-cones. The 480-nm background served to suppress the rods, but also selectively desensitized the M-cones. Consequently, these conditions isolate the L-cone response over most of the 6.5 to $11.5 \log_{10} \text{ quanta s}^{-1} \text{ deg}^{-2}$ range of target intensities. However at the highest intensities the M-cones are also likely to contribute to flicker detection; we were not concerned about the possibility of mixed M- and L-cone detection at those levels. Only cff measurements were made for L-cone-detected flicker.

Procedures

All observers light adapted to the background and target for 3 minutes before measurements began. They interacted with the computer controlling the experiment by means of an eight-button keypad, and received information and instructions via tones and a computer-controlled voice synthesizer. Each measurement was the average of at least three settings and the experiment was repeated two or three times, usually on separate days. For a few measurements, noted below, only one repeat of the measurements could be made. The visual stimulus, focused in the plane of the pupil, was the only visible light source for the observers in an otherwise dark room. The image of the source in the plane of the observers' pupils was always less than the minimal pupil size so that retinal illumination was not affected by pupil size. The method of adjustment was used in measuring the cff, temporal contrast-sensitivity functions (TCSFs), and phase delays.

Calibration

The radiant fluxes of test and background fields were measured at the plane of the observer's entrance pupil with a UDT Radiometer that had been calibrated against a standard, traceable to the National Bureau of Standards. Neutral density filters, fixed and variable, were calibrated *in situ* for all

test and field wavelengths used. Interference filters were calibrated *in situ* with a spectroradiometer (Gamma Scientific). All radiances are given as time-averaged values.

EXPERIMENT I: Critical flicker fusion measurements

Introduction

In the first experiments, we measured the cff for S-cone- and L-cone-detected flicker to gauge the temporal acuity limits and relative sensitivities of ESCS observers compared with normals.

Methods

All six ESCS observers participated in the S-cone cff measurements, ES1-ES4 participated in the L-cone cff measurements.

For the S-cone measurements, a 440-nm target was presented in the centre of steady, 620-nm background field of $11.41 \log_{10} \text{ quanta s}^{-1} \text{ deg}^{-2}$, and the target radiance was varied from 6.30 to $11.00 \log_{10} \text{ quanta s}^{-1} \text{ deg}^{-2}$ in steps of about 0.3 \log_{10} unit. For the L-cone measurements, a 650-nm target was presented in the centre of a steady, 481-nm background field of $8.26 \log \text{ quanta s}^{-1} \text{ deg}^{-2}$, and the target radiance was varied from 6.50 to $10.50 \log_{10} \text{ quanta s}^{-1} \text{ deg}^{-2}$ in steps of about 0.3 \log_{10} unit.

At each target radiance, observers adjusted the flicker frequency (at the fixed maximum stimulus modulation of 92%) using the method of adjustment to find the frequency at which the flicker just disappeared. Observers were instructed to approach the cff from both lower and higher frequencies.

During a single run of the experiment, three settings were made at each radiance and averaged. The experimental runs were repeated on three separate occasions, except for ES5 (one occasion) and ES6 (two occasions).

Results

S-cone critical flicker fusion measurements

The six panels of Figure 1 show the S-cone cff (temporal acuity) data for the six ESCS observers (ES1 to ES6, coloured circles) plotted as a function of \log_{10} target radiance. For comparison, the

mean cff data for 12 normal control subjects are also plotted in each panel (blue squares). The error bars in all figures are ± 1 standard error of the mean (s.e.m.) within observers for the ESCS measurements, and between observers for the normal measurements. The small open circles are shifted ESCS data and their significance will be discussed later.

[Insert Figure 1 about here]

In the normal observer, S-cone cff rises steadily from just above a radiance of $6.5 \log_{10}$ quanta $s^{-1} \text{ deg}^{-2}$ until about $9.0 \log_{10}$ quanta $s^{-1} \text{ deg}^{-2}$, after which it reaches a plateau and decreases slightly. This decrease may result partly from saturation of the S-cone signal³¹ but is also due, in part, to chromatically-opponent interactions with the other cone types.^{31, 49, 50} The rise in cff above about $9.9 \log_{10}$ quanta $s^{-1} \text{ deg}^{-2}$ in normal observers is due to flicker detection by M-cones (see Figure 4 of Stockman & Plummer³¹).

Below about $9.0 \log_{10}$ quanta $s^{-1} \text{ deg}^{-2}$, the ESCS cff functions have similar slopes to the mean normal function. Above $9.0 \log_{10}$ quanta $s^{-1} \text{ deg}^{-2}$, however, the shapes of the ESCS cff functions show sizable individual differences, which we consider in the Discussion.

L-cone critical flicker fusion measurements

The four panels of Figure 2 show the mean L-cone critical flicker fusion frequencies for four ESCS observers (ES1 to ES4, coloured circles), again plotted as a function of \log_{10} target radiance. For comparison, the mean cff data for 12 normal control subjects are plotted in each panel (dark red squares). The error bars are ± 1 standard error of the mean (s.e.m.) within observers for the ESCS measurements, and between observers for the normal measurements.

[Insert Figure 2 about here]

In the normal observer, L-cone cff rises steadily from just above $6.5 \log_{10}$ quanta $s^{-1} \text{ deg}^{-2}$ until about $9.0 \log_{10}$ quanta $s^{-1} \text{ deg}^{-2}$, after which the cff approaches a plateau near 40 Hz.^{51, 52} The L-cone cff functions for the four ESCS observers (coloured symbols) all show losses in cff of varying degrees relative to that for normal observers. ES1 shows the greatest loss and ES2 the least. The slopes of the cff functions are also variable. Compared to the slope of the normal cff, those for ES2 and ES3 are shallower, whereas those for ES1 and (possibly) ES4 are similar to the normal slopes. The L-cone cff functions for ES1, ES2, ES3 and ES4 reach 29, 35, 30 and 31 Hz, respectively, compared to 40 Hz for the normal function.

Discussion

The S-cone and L-cone cff data for ESCS observers are broadly consistent with the work described in the Introduction and show both improvements in S-cone sensitivity and reductions in L- and M-cone sensitivities.^{2, 3, 8-10}

All ESCS observers show some improvements in S-cone cff relative to the mean normal observer. This is a notable feature of ESCS, where despite the progressive retinal degeneration, there is a specific gain in visual function. Two of the observers (ES1 and ES6) show relatively small improvements in S-cone cff. Although this might seem at odds with their diagnosis, S-cone sensitivity improvements can be greater at frequencies below the cff, as the next experiment illustrates. For instance, although ES1 shows only a small improvement in S-cone cff relative to the mean normal observer (see Figure 1), ES1 shows clear improvements in contrast sensitivity between 7.5 and 20 Hz at high radiance levels (see Figure 3, below).

The shapes of the ESCS cff functions show sizable individual differences above $9.0 \log_{10}$ quanta $s^{-1} \text{ deg}^{-2}$. Those for ES1, ES2 and ES5 reach a plateau at about 30 Hz—well above the 22-Hz plateau of the normal observers—but show none of the subsequent increase in performance attributed in normals to M-cone intrusion. In contrast, the function for ES6 shows a substantial loss of cff above $9.5 \log_{10}$ quanta $s^{-1} \text{ deg}^{-2}$, which is difficult to interpret because of the variability in ES6's measurements at these high radiance levels. The data for ES4 and particularly ES3 continue to rise at high target radiances, perhaps because, in normal observers, the interactions between S-cones and L- and M-cones that contributes to their 22-Hz plateau is weaker. We assume that the differences in cff at radiances above $9.0 \log_{10}$ quanta $s^{-1} \text{ deg}^{-2}$ both between the ESCS observers and between them and the mean normal observer partially reflect individual differences in the strengths of signals from the L- and M-cones. In this region, the L- and M-cones are implicated in limiting the effectiveness of the S-cone signals,^{31, 49, 50} and in normal observers the M-cones take over flicker detection at the highest radiances.³¹

As can be seen in Figure 2, the L- and M-cone loss is greater for some ESCS observers than others. This implies, perhaps, that the influence of the L- and M-cones on the S-cone cff at the highest levels is likely to be much less for ES1 than for ES2.

Consistent with earlier measurements,^{2, 8, 9} all four of the ESCS observers who made L-cone cff measurements show some loss in cff sensitivity (see Figure 3), but the extent and form of the loss varies between observers, making simple interpretation difficult.

EXPERIMENT II: S-cone temporal contrast sensitivity measurements

Introduction

S-cone temporal contrast-threshold functions (TCSFs) were measured at three mean radiance levels to assess the temporal responses of the ESCS observers at frequencies below cff, and to compare them with the normal response.

Methods

Only ES1, ES2 and ES3 were available to participate in these experiments. Measurements were made at three time-averaged 440-nm target radiances: 7.40 (low), 8.73 (medium) and 9.61 (high) \log_{10} quanta $s^{-1} \text{ deg}^{-2}$. As for the cff measurements, the 440-nm targets were presented in the centre of steady, 620-nm background field with radiance fixed at 11.41 \log_{10} quanta $s^{-1} \text{ deg}^{-2}$.

At each target frequency, observers adjusted the flicker contrast using the method of adjustment to find the contrast at which the flicker just disappeared. Observers were instructed to approach the threshold contrast from both below and above threshold.

During a single run of the experiment at one of the mean target radiances, three threshold settings were made at each flicker frequency and then averaged. The experimental runs were repeated on two or three separate occasions, depending on observer availability.

Results

The results are shown in the nine panels of Figure 3. Each panel illustrates the mean \log_{10} S-cone contrast threshold plotted as a function of frequency (logarithmic axis). The upper, middle and bottom rows show data for the high (9.61 quanta $s^{-1} \text{ deg}^{-2}$), medium (8.73 quanta $s^{-1} \text{ deg}^{-2}$) and low (7.40 \log_{10} quanta $s^{-1} \text{ deg}^{-2}$) target radiances, respectively. The left-hand, middle and right-hand columns show data for ES1 (yellow symbols), ES2 (red symbols) and ES3 (green symbols), respectively. The blue squares in each panel show the mean results of 12 normal observers. The error bars in all figures are ± 1 standard error of the mean (s.e.m.) within observers for the ESCS measurements, and between observers for the normal measurements. In many cases, the error bars are smaller than the symbols.

[Insert Figure 3 about here]

The mean normal data (blue squares) are low-pass in shape at all radiances—that is they are constant at low temporal frequency and fall only at higher frequencies. In contrast, the data for ES1, ES2 and ES3 are low-pass only at the lowest target radiance; at the medium and high radiances they are band-pass in shape, peaking in sensitivity near 7.5 Hz, and falling off at both lower and higher frequencies. At the two higher radiance levels, performance of the ESCS observers is as good as, and, in 5 out of 6 cases, much better than, that of the normal observers. The model fits shown by the red continuous lines will be described in the General Discussion.

Discussion

The temporal contrast sensitivity data shown in Figure 3 provide new details about the ESCS phenotype. At the medium and high 440-nm target level, the contrast sensitivities for the ESCS observers, unlike those for normal observers, are clearly band-pass in shape peaking at 7.5 Hz. Low-frequency attenuation is usually attributed to a sluggish or delayed surround antagonism^{53, 54}, so one possibility is that higher S-cone density in ESCS observers results in greater S-cone surround antagonism between neighbouring S-cones perhaps via horizontal, H2 cells, which have mixed inputs from all three cone types.⁵⁵ The normal density of S-cones reaches about 2000 cells mm⁻² (about 8% of the cone population) within the area of the target (see Table 1 of Calkins⁵⁶). Consequently, any increase in density will increase the number of S-cones likely to be contacted by each H2 horizontal cell^{55, 57, 58} and thus will potentially increase the S-cone surround signal.

However, the results in Figure 3 show that at the medium and high levels the high-frequency slope on these double logarithmic co-ordinates is steeper for the ESCS observers than for the mean normal observer. A very sluggish surround signal is unlikely to cause steepening at high frequencies, which suggests that the interaction may be between the normal S-cone signal and a faster S-cone signal that destructively interferes not only at low frequencies, but also at high frequencies. A model, the predictions of which are shown by the red continuous lines in Figure 3, is presented in the General Discussion.

We note that although the mean temporal contrast sensitivity functions (blue squares, Figure 3) are low-pass in shape, the shapes of underlying individual functions vary. In particular, two of the normal observers show low-frequency attenuation comparable to that found in the ESCS observers. We speculate that these observers have higher than average S-cone densities, so that their results are more similar to those of ESCS observers.

EXPERIMENT III: S-cone phase delay measurements

Introduction

Under intense long-wavelength adaptation, S-cone-detected flicker of the appropriate phase will cancel or null L/M-cone-detected flicker, suggesting that under those conditions the signals are transmitted by a common luminance pathway.^{28, 46} This type of cancellation is known as “flicker-photometric cancellation”. Because cancellation between S-cone detected flicker and L/M detected flicker occurs, not only the relative size of the S- and L/M-cone responses can be determined, but also the relative delay and sign of the S-cone signal within the common pathway.

Methods

Only ES1, ES2 and ES3 were available to participate in these experiments.

Phase delay measurements were made at the medium S-cone level between S-cone-detected flicker and L/M-cone detected flicker. The S-cone-detected flicker was generated by the fixed 440-nm 4° diameter target of $8.73 \log_{10} \text{ quanta s}^{-1} \text{ deg}^{-2}$ presented in the centre of the steady, 620-nm background field of $11.41 \log_{10} \text{ quanta s}^{-1} \text{ deg}^{-2}$. The L/M-cone-detected flicker was generated by a 4° diameter 610-nm target superimposed on the 440-nm target. Its radiance, viewed alone on the 620-nm background, was adjusted by the observer so that 15-Hz flicker at the maximum 92% modulation was just visible (this ensured that the 610-nm target was at the radiance necessary for the experiment, and was always much dimmer than the background). The 610-nm target radiances in $\log_{10} \text{ quanta s}^{-1} \text{ deg}^{-2}$ were 10.32 for ES1, 9.95 for ES2, and 10.04 for ES3.

The S-cone and the L/M-cone targets were flickered at frequencies between 2.5 and 15 Hz in 2.5-Hz steps. The two targets were initially presented in opposite phase, but their relative phase and strength of modulation could be adjusted by the observer or by the experimenter to find the relative phase and modulation strength at which the flicker appeared nulled or had a clear minimum (i.e., when the summed flickering targets appeared to cancel each other). The initial adjustments of phase for the three ESCS observers were carried out by the experimenter, who was unaware of the absolute phase delay, but aware of the relative changes in phase that could be made by pressing various keys (steps of 2, 10 and 180°). By asking the observer whether he or she could see more flicker in one phase condition versus another, it was possible for the experimenter to quickly determine to within about 10° the relative phase that produced the best null. Fine adjustments could then be made by the observer. This interactive approach proved successful and circumvented

the need for much more extensive training, which was not feasible given the limited availability of the ESCS observers.

A single interactive run of the experiment was carried out.

[Insert Figure 4 about here]

Results

The coloured circles in each of the three panels of Figure 4 show the S-cone phase delays (in degrees) for ES1, ES2 and ES3 (yellow, red and green circles, respectively) plotted as a function of frequency (both axes linear).

For comparison, the mean results for five normal observers (blue diamonds) are plotted in each panel. The mean function for normal observers follows a roughly straight line, the extrapolation of which crosses the y-axis (0 Hz) at -180° . Note that the normal observers' error bars are fairly large, which reflects the variability in the underlying data. The significance of the solid red, green and blue lines will be described later.

The phase delay data for the three ESCS observers show some variability. The data for ES1 (yellow circles) lie substantially above the normal mean data, but those for ES2 (red circles) and ES3 (green circles) are closer. The differences between the phase delays for ES2 and the normal observers are relatively small, but the phase delays for ES3 are consistently above the normal function and have a different slope.

Discussion

The mean normal S-cone phase delays are consistent with a time delay between the L/M-cone signals of Δt ms, and a signal inversion. Thus, the phase delay in $\Delta\theta$ (degrees) as a function of f (frequency in Hz) can be written:

$$\Delta\theta(f) = 360\Delta t f + 180. \quad [3]$$

where the addition of 180° represents (and has the same effect as) signal inversion or inhibition. The blue lines fitted to the normal data are the best-fitting version of a pure delay model defined by Equation [3] for which $\Delta t = 39.57 \pm 0.59$ ms ($R^2 = 0.991$). Thus, as expected, the phase delays of the normal observers are consistent with a time delay and sign inversion.^{28, 44-46}

The deviations of the ESCS data from the normal data in Figure 4 potentially yield insights into differences between the normal and ESCS in the postreceptoral organization of the S-cone signal. A

model, the predictions of which are shown by the red lines in each panel of Figure 4, is developed in the General Discussion.

The fact that ESCS observers, like normal observers, can cancel 440- and 610-nm flicker on a 620-nm background suggests that against that background the S-cone and L/M-cone signals for the ESCS observers are also transmitted by a common pathway, the properties of which are consistent with those of the luminance channel.²⁸

GENERAL DISCUSSION

The psychophysical results for the ESCS observers reveal clear differences between their data and the mean normal data. In this section, we endeavour by analysis and modelling to interpret the differences in terms of changes in cone density or in postreceptoral organisation.

Enhancements of S-cone cff and increases cone density

Up to about $9.0 \log_{10}$ quanta $s^{-1} \text{deg}^{-2}$, the enhancements in S-cone cff for the ESCS observers are approximately consistent with simple vertical shifts of the normal cff function to higher frequencies (see Figure 1). We can therefore use these shifts to quantify the relative improvement for each ESCS observer. Accordingly, we determined the vertical shift in cff that minimized the squared differences between the ESCS and normal cff functions below $9.0 \log_{10}$ quanta $s^{-1} \text{deg}^{-2}$. The best-fitting shifts and \pm the standard errors are 1.14 ± 0.33 , 5.30 ± 0.27 , 2.58 ± 0.22 , 6.25 ± 0.25 , 4.77 ± 0.12 and 0.85 ± 0.65 Hz for ES1 to ES6, respectively, with R^2 values of 0.974, 0.981, 0.989, 0.985, 0.997 and 0.902. The shifted ESCS data are shown in each panel of Figure 1 by the small open circles superimposed on the normal data. The sizes of the standard errors show that significant enhancements in cff are found for five of the six ESCS observers. In the Appendix of this paper, we develop a metric that enables the shift in cff to be translated into an estimate of the change in photoreceptor number.

The analysis on which the metric is based, equates changes in cone number caused by changing target area with changes in cone number caused by photoreceptor gain or loss *within* a fixed target area (see Equation A4). Using this equation, we can estimate the factor by which the cone number increases that corresponds to the vertical shift in cff that we find for each observer. The factors we infer are increases by 1.56, 7.83, 2.72, 11.32, 6.37 and 1.39 for ES1, ES2, ES3, ES4 ES5 and ES6, respectively. These factors are much less than the increase of 75 times estimated from ERG

measurements,⁹ but we emphasize that these approximations are dependent on several assumptions (see Appendix).

S-cone temporal contrast threshold measurements and signal interactions

The shapes of the S-cone ESCS contrast sensitivities (see Figure 3) suggest that two S-cone signals interact in a way that lowers sensitivity at both high and low frequencies but raises it at intermediate frequencies. We model this interaction by assuming that there are two S-cone signals: a fast “centre” signal, $A_c(f)$, and a second inhibitory “surround” signal, $A_s(f)$, that is delayed by Δt ms. Given a fixed time delay, the phase delay in $\Delta\theta$ (degrees) as a function of f (frequency in Hz) is given by Equation [3] above (but between two S-cone signals rather than between S-cone and L/M-cone signals).

The resultant signals produced by adding together $A_c(f)$ and $A_s(f)$ at the angles determined by their relative (frequency dependent) phase differences (Equation [3]) is then:

$$A_r(f) = \sqrt{(A_c(f) + A_s(f) \cos[\Delta\theta(f)])^2 + (A_s(f) \sin[\Delta\theta(f)])^2}. \quad [4]$$

Figure 5 illustrates the vector addition of A_c (open arrow) and A_s (grey arrow) separated by a relative phase delay of $\Delta\theta(f)$ (red arc). Their addition yields the resultant vector A_r (black arrow), which has a phase delay of ϕ relative to A_c (green arc). (The component of A_s in the direction of A_c [$A_s \cos(\Delta\theta)$] and the component at right angles to A_c [$-A_s \sin(\Delta\theta)$] are shown as thin black lines.)

[Insert Figure 5 about here]

The model defined by Equations [3] and [4] was fitted to the ESCS data of Figure 3. Various schemes were tried for determining the shapes of $A_c(f)$ and $A_s(f)$. Somewhat surprisingly, however, we found that at the medium and high levels we could simplify the model by assuming that *both* $A_c(f)$ and $A_s(f)$ were similar in shape to the mean normal function (blue squares, Figure 3)—and that they differed only by a scaling constant (such that $A_c(f) = wA_s(f)$, where w is the relative weight of the centre signals [thus, the vector length $A_c(f)$ in Figure 5 and Equation [4] becomes $wA_s(f)$]). The model fits based on this assumption are shown by the continuous red lines in Figure 3. An additional logarithmic scaling constant, s , that simply shifts the fitted functions up or down was also allowed in the fitting procedure. Since, in preliminary fits, the delay Δt was similar across ESCS observers at the high and medium levels, we constrained it to have the same value for all three observers at these levels.

The fits at the low level were different. The data for ES2 and ES3 were similar in shape to the mean normal S-cone contrast sensitivity function without an additional second signal. Thus for them,

w at the low level was fixed at 0. For ES1, a second signal was required but since the delay Δt was poorly constrained (and tended towards either very small or very high values), we fixed it at the mean of ES1's best-fitting values obtained at the high and medium levels.

TABLE 1

		ES1	ES2	ES3
High	Delay (ms)	37.49±1.46		
	w	0.37±0.12	0.24±0.12	0.63±0.16
	s	0.25±0.04	0.25±0.03	0.51±0.04
	R^2	0.924		
Medium	Delay (ms)	44.93±1.18		
	w	0.36±0.08	0.23±0.07	0.43±0.05
	s	0.02±0.02	0.30±0.02	0.27±0.02
	R^2	0.981		
Low	Delay (ms)	41.21*	--	--
	w	0.38±0.17	0*	0*
	s	-0.23±0.05	-0.06±0.05	0.13±0.04
	R^2	0.913		

Best-fitting versions of the model were obtained using a standard non-linear, least-squares curve-fitting algorithm (implemented in SigmaPlot, SPSS). The best-fitting parameters and their standard errors are given in Table 1, along with the R^2 values for the fits at each radiance level. The fits, shown by the red continuous lines in each panel of Figure 3, are good, having R^2 values of 0.913 or better. Fixed values are noted in Table 1 by the asterisks. The values of s capture the individual differences in frequency-independent overall sensitivity.

The model and fits are intended to be largely illustrative. Although they clearly demonstrate that the ESCS contrast sensitivity data are consistent with an interaction between two similar S-cone signals of opposite sign, one of which is delayed relative to the other, the details of the model are less secure. For example, the simplification that the two signals have the same dependence on frequency is unlikely to be precisely correct. More sluggish signals are usually subject to some form of filtering that causes more attenuation at high frequencies.⁵⁹ And, we find that slightly better fits can be obtained at the high and medium levels by filtering the slow signal at these levels with a single-stage low-pass filter with a corner frequency of about 6 and 11 Hz, respectively.

Given that we assume that $A_c(f)$ and $A_s(f)$ are of the same shape, we cannot determine from the fits which of them is bigger, since, in principle, because of symmetry, w could be applied either to $A_s(f)$ or to $A_c(f)$. In the model, we assume that $A_c(f)$ is smaller than $A_s(f)$ (so $w < 1$) on the grounds that the S-cone phase delays (see Figure 4 and the next section) suggest that the sign of the S-cone resultant signal is negative [which implies that when $\Delta\theta = 180$, at 0 Hz, $A_s(f) > A_c(f)$].

S-cone phase delays and signal interactions

The analysis in the previous section suggests that two S-cone signals separated by a delay interact in the ESCS observer to produce the bandpass temporal contrast sensitivity functions of Figure 3 at the medium and high levels. One of these signals is likely to be the S-cone signal also found in normals, which is delay and inverted in sign (shown by the blue diamonds, Figure 4). Conceivably, the second signal could be more delayed than the normal signal, in which case it might be a surround signal, or it could be less delayed, in which case it might be a more direct S-cone signal that avoids the normal S-cone pathway. The green lines in Figure 4 illustrate the expected phase delays if there were only a fast signal with the same delay as the L/M-cone signal and this prediction clearly does not fit the data.

We modelled the S-cone phase delay data by assuming, as before, that there are two S-cone signals $A_c(f)$ and $A_s(f)$ of opposite sign and separated by a time delay of Δt ms (as in Equation [3]). The phase delay of the resultant S-cone signal (see Figure 5), $\phi(f)$ is:

$$\phi(f) = \tan^{-1} \left[\frac{A_s \sin \Delta\theta}{A_c + A_s \cos \Delta\theta} \right] \quad [5]$$

Again, if we assume that $A_c(f) = wA_s(f)$, so that $w = A_c(f)/A_s(f)$, Equation [5] simplifies to:

$$\phi(f) = \tan^{-1} \left[\frac{\sin \Delta\theta}{w + \cos \Delta\theta} \right]. \quad [6]$$

The model defined by Equations [3] and [6] was fitted individually to the S-cone phase delays for each ESCS observer and the fits are shown as red lines in Figure 4. The best-fitting parameters and their standard errors are given in Table 2, along with the R^2 values.

The fits for ES2 and ES3 are good. Moreover, the delays between the two S-cone signals for the two observers are comparable to the delay of 44.93 ms inferred from the temporal contrast sensitivity data at the same level (see Table 1); the values of w agree less well. The continuous black lines shown in Figure 4 are the phase predictions from the model used to account for the temporal contrast sensitivity functions, which are plausible for ES2 and ES3. The fits for ES1, however, agree

much less well. Indeed, the requirement of the phase model—that the two S-cone signals should be equal in size and should therefore cancel each other when they are in opposite phase (at 0 and 15 Hz)—is clearly inconsistent with ES1’s temporal contrast sensitivity data, which show much less attenuation at those frequencies. We do not understand the cause of this discrepancy. Note that when $w = 1$, as in the best fit for ES1, Equation [6] simplifies to $\phi(f) = \Delta\theta / 2$ (red line, upper panel, Figure 4).

TABLE 2

	ES1	ES2	ES3
Delay (ms)	66.66±5.38	41.10±3.19	44.60±1.49
w	1.000±0.18	0.00±0.30	0.78±0.15
R^2	0.818	0.881	0.970

Conclusions

On balance, the phase and contrast-sensitivity models suggest that two S-cone signals generate S-cone flicker in the ESCS observer under long-wavelength adaptation. The larger S-cone signal is comparable to the slow, inverted S-cone signal found in normal observers. The second, smaller S-cone signal reduces the S-cone phase delays (relative to L/M-cone flicker), which suggests that it is a faster, positive signal more similar to the L/M-cone signals against which the S-cone phase delays are measured.

The existence of “normal” S-cone pathways in the ESCS observer is supported by other work. ESCS patients, for instance, are also affected by the phenomenon of transient tritanopia (the loss of S-cone sensitivity following the offset of a yellow field, see Mollon⁶⁰), which is also consistent with a normal, spectrally-opponent postreceptoral organization of S-cone signals.³ Given that in the “normal” S-cone pathways the signals from S-cones are opposed by signals from M- and L-cones (for reviews, see Mollon⁶¹ and Calkins⁵⁶), improvements in chromatic S-cone sensitivity in ESCS observers could be due in part to a reduction in the number of L- and M-cones.

This evidence for a faster S-cone signal in ESCS both from the temporal contrast sensitivity measurements at the medium and high levels, and from the S-cone phase delay measurements does not address the issue of how such a fast signal arises. One possibility is that some of the abundant S-cones in ESCS observers displace the direct L- and M-cone inputs into the luminance pathway, thus giving rise to a fast, positive S-cone luminance signal. However, if S-cones do feed prominently into faster L- and M-cone pathways, then a faster response should be evident in the ERG. Yet, although

the leading edge of the a-wave is similar to other cone responses,⁹ the b-wave of the S-cone response is substantially delayed in these observers as it is in normal observers.³ The normal leading edge of the a-wave yet anomalous b-wave are consistent with the S-cones in the central macula region feeding through the normal S-cone pathways⁴, although rod pathways may be involved in the periphery.⁴ Indeed, one possibility is that the “fast” S-cone signals in our measurements are transmitted via sluggish rod pathways, which would explain why the relative amplitudes of the fast and slow S-cone signals required to model the temporal contrast-sensitivity functions are not more dissimilar. However, it would not explain their phase characteristics, which, unlike rod signals, show relatively little delay (see above).

We note that comparisons between the postreceptoral organization of the ESCS and normal retina may not be straightforward. Substantial rewiring can occur after photoreceptor degeneration,^{62, 63} so that the faster S-cone signal in ESCS may be transmitted through a novel pathway that has no normal counterpart.

If the S-cones in ESCS observers have access to normal L- and M-cone pathways, or even if there are simply more S-cone pathways to match the increase in S-cone number, then we should expect improvements in S-cone spatial contrast-sensitivity and spatial-acuity measures. Unfortunately, the most relevant evidence from Greenstein *et al.*¹⁰ is equivocal at best, since it shows very modest improvements in spatial acuity. The maximum spatial acuities for their ESCS observers P2 and P3 reach about 6 cycles per deg (cpd), and for their observer P1 about 10 cpd (see their Figure 5). By contrast, the maximum normal S-cone acuity reported by Humanski and Wilson⁶⁴ is 4 cpd, and as yet unpublished spatial contrast-sensitivity measurements from our laboratory suggest S-cone mediated spatial-acuity limits in normal observers can be as high as 7 to 10 cpd. (These values should be contrasted to comparable L- and M-cone spatial acuity limits, which can be as high as 55 cpd.⁶⁵)

APPENDIX

The question we address here is how the shifts in S-cone cff might be usefully related to increases or decreases in photoreceptor number. We start with a useful approximation for targets of between about 1° and 5° of visual angle in diameter first noted by Granit and Harper that cff increases linearly with the logarithm of the target area⁶⁶. See Figure 1 of Kugelmass & Landis⁶⁷ for a graphical summary of relevant results up to 1955. Here, we take advantage of the detailed set of cff measurements made by Kugelmass & Landis⁶⁷ as function of both target luminance and area, for which the Granit-Harper law is approximately obeyed for foveally-fixated target diameters of

between 3° and 7° of visual angle (see Figure A, upper panel). These form part of an extensive historical literature on cff measurements (for reviews, see Simonson & Brožek⁶⁸ and Landis⁶⁹) that dominated research on temporal processing before linear systems theory and measurements of temporal contrast sensitivity of sinusoidally flickering stimuli became common in the late 50's and early 60's.^{37, 70, 71} More recent work that nicely links cff to linear systems theory has been carried out in several studies by Tyler and Hamer.^{25, 72-74}

We relate the changes in area to the changes in the number of cones underlying the target by a theoretical analysis of data that links changes in cff to changes in cone number. A similar approach that linked cff to ganglion cell number over the whole retina was developed by Rovamo & Raninen.⁷⁵ The upper panel of Figure A shows mean cff (linear) as a function of the logarithm of target area ($\log_{10} \text{deg}^2$) for targets between 1.27° and 14.60° in visual diameter from Table 1 (columns “for the average results of ES and SK”) of Kugelmass & Landis⁶⁷ and plotted in the upper part of their Figure 3 as open symbols. Their targets were circular, centrally fixated, and the flicker waveform was square-wave. Data are shown for luminance levels of 1.24 (blue diamonds), 1.64 (cyan inverted triangles), 2.44 (green squares), and 3.64 (red circles) log photopic trolands (phot. td). (Converted from mL assuming a 2-mm pupil diameter.)

[Insert Figure A about here]

The cff data have been vertically aligned with their mean using the data between target diameters of 2.98° and 7.10° over four luminances: vertical shifts of 10.81, 6.55, -4.13, -10.05 and -13.23 Hz for the cff data for 1.24, 1.34, 2.44, 3.04 and 3.64 log phot. td levels, respectively. The alignment minimized the squared differences between each data set and the mean. (The vertical red lines indicate target diameters of 2.98° and 7.10° between which the fit was made and 4.00°, and which includes the size used in our experiments.)

The data between 2.98° to 7.10° of visual angle are seen to be differentiated only by a (vertical) shift in cff so that the *shape* of the function relating cff to retinal area is approximately independent of luminance level. The straight line (black line in the upper panel) fitted to the aligned data between 2.98° and 7.10° has the formula:

$$\text{cff} = 3.50 \log_{10} A + 24.78, \quad [\text{A1}]$$

where A is the area in deg^2 . The R^2 for the fit is 0.860. The dashed lines show the fitted line extended outside the fitted range.

Next, we need to convert target area in deg^2 to cone number. To make the conversion, we used the human cone-density estimates for temporal retina made by Curcio *et al.*,⁷⁶ which we have

replotted in Figure B as yellow circles. Using a curve discovery program (TableCurve 2D, Jandel Scientific), we generated an arbitrary continuous exponential function that fit the Curcio *et al.* data from 0 to 60° with an R^2 of 0.998. The function fitted to the Curcio *et al.* data shown by the red line in Figure B was generated to provide a continuous function of cone density versus eccentricity. The function is:

$$\text{density} = e^q, \quad q = \frac{a+c\varepsilon+e\varepsilon^2+g\varepsilon^3}{2.303+b\varepsilon+d\varepsilon^2+f\varepsilon^3}, \quad [\text{A2}]$$

where the density is in cones per deg², ε is the eccentricity in deg, $a = 9.570$, $b = 3.839\text{e-}1$, $c = 1.866$, $d = -1.343\text{e-}2$, $e = -6.504\text{e-}4$, $f = 4.464\text{e-}3$ and $g = 2.295\text{e-}2$.

[Insert Figure B about here]

We then used this function to calculate the number of cones in successive annular rings with inner and outer diameters differing by 0.01° for inner diameters between 0 and 60° of eccentricity also in steps of 0.01°. The cone numbers for each of the particular targets used by Kugelmass & Landis⁶⁷ were then calculated using the continuous exponential function by summing the cone numbers in all the annular rings that made up each target. These calculations enabled us to plot the cff against cone number instead of the retinal area. The lower panel of Figure A shows the aligned cff data from between 2.98 and 7.1° from the upper panel plotted as a function of the logarithm of the number of cones. [Tyler⁷⁷ accounted for comparable cone density data from Oesterberg⁷⁸ with a logarithmic slope of -0.667 for eccentricities between 0.1 and 15°. This function can also plausibly account for the Curcio data between 0.1 and 15°, but substantially overestimates cone densities below 0.1°; the densities below 0.1° are needed to estimate cone number for centrally-fixated targets.]

The aligned cff data plotted in the lower panel can also be approximated by a straight line (black line), the formula for which is:

$$\text{cff} = 5.93 \log_{10} N + 0.96, \quad [\text{A3}]$$

where N is the number of cone photoreceptors. The R^2 for the fit is 0.861. Thus, for a change in cff of Δcff Hz, the change in the ratio of the number of cones, r , is given by:

$$r = 10^{\frac{\Delta\text{cff}}{5.93}}. \quad [\text{A4}]$$

Equation [A4] is independent of the absolute cff over the range 17 to 43 Hz and of the luminance level over the range 1.24 to 3.64 log phot. td, and provides an estimate of the relative change in cone density. The absolute cone densities can be calculated using Equation [A4] for the target size used in our experiments. Consequently, for ESCS observers, for whom the vertical shifts in cff

increased by between 0.85 and 6.25 Hz (see above) we estimate the increase in S-cone number to be between 1.39 and 11.32 times normal.

Equation [A4] provides a useful indication of the approximate relative increase or decrease in photoreceptor number with cff. However, we stress that the approximation is inevitably limited most obviously to the range of target diameters from about 3 to 7° over which the Granit-Harper law holds (see above). Implicit, too, in the approximation is the assumption that both the effective quantum catch and the temporal characteristics of the cones remains constant as their density varies between eccentricities of 1.59 and 3.55°. This assumption is likely to be only approximate, although the result that the cone photopigment optical density measured psychophysically is roughly constant over this range⁷⁹ suggests some uniformity.

Another useful approximation for accounting for cff results is known as the Ferry-Porter “law”, which holds that for intermediate luminance levels the growth of cff is proportional to the logarithm of the luminance (that is, a plot of cff versus log luminance should have a linear slope).^{80, 81} Of relevance in this context are observations that the proportionality constant and thus the cff increases as a function of eccentricity (under conditions where the same number of cones are stimulated at each eccentricity).^{25, 74} This change is evident in the data shown in Figure A, in which the slope of the underlying cff versus target luminance functions must be shallower below a target diameter of 2.98° than between diameters of 2.98 and 7.10°. Obedience to the Granit-Harper law between 2.98 and 7.10° suggests, however, that the Ferry-Porter proportionality constant for these targets must be roughly constant. Nevertheless, we acknowledge that the variation of the Ferry-Porter slope with eccentricity may be a confounding factor.

A complication in relating cff to changes in cone number in clinical populations is that reductions in cff can also arise when disease or mutations disrupt normal photoreceptor sensitivity regulation. However, since such photoreceptor impairment is likely to result in a change in the slope of the cff versus luminance function rather than a simple vertical shift, it may be possible to some extent to disambiguate photoreceptor impairment from loss. Further discussion of photoreceptor sensitivity regulation and temporal sensitivity can be found in our earlier papers.⁸²⁻⁸⁴

ACKNOWLEDGEMENTS

This work was supported by grants from Fight for Sight, BBSRC, EPSRC and the National Institute for Health Research Biomedical Research Centre at Moorfields Eye Hospital NHS Foundation Trust

and UCL Institute of Ophthalmology. ARW and ATM are supported a Foundation for Fighting Blindness Research Center grant for the Study of Retinal Degenerative Diseases. MM is supported by a Foundation Fighting Blindness Career Development Award. We especially acknowledge the help of the ESCS observers who participated in this study without whom this work would not have been possible.

REFERENCES

1. Marmor MF, Jacobson SG, Forester MH, Kellner U, Weleber RG. Diagnostic findings of a new syndrome with night blindness, maculopathy, and enhanced S cone sensitivity. *American Journal of Ophthalmology* 1990;110:124-134.
2. Jacobson SG, Marmor MF, Kemp CM, Knighton RW. SWS (blue) cone hypersensitivity in a newly identified retinal degeneration. *Investigative Ophthalmology & Visual Science* 1990;31:827-838.
3. Kellner U, Zrenner E, Sadowski B, Foerster MH. Enhanced S cone sensitivity syndrome: long-term follow-up, electrophysiological and psychophysical findings. *Clinical Vision Sciences* 1993;8:425-434.
4. Marmor MF, Tan F, Sutter EE, Bearse Jr MA. Topography of cone electrophysiology in the Enhanced S-cone syndrome. *Investigative Ophthalmology and Visual Science* 1999;40:1866-1873.
5. Gouras P, MacKay CJ, Evers H, Eggers HM. Computer assisted spectral electroretinography (CASE): a tool for examining hereditary retinal degenerations. In: Vail MM, Hollyfield JG, Anderson RE (eds), *Retinal degeneration Experimental and clinical studies*; 1985:115-130.
6. Fishman GA, Peachey NS. Rod-cone dystrophy associated with a rod system electroretinogram obtained under photopic conditions. *Ophthalmology* 1989;96:913-918.
7. Marmor MF. Large rod-like photopic signals in a possible new form of congenital night blindness. *Documenta Ophthalmologica* 1989;71:265-269.
8. Román AJ, Jacobson SG. S cone-driven but not S cone-type electroretinograms in the enhanced S cone syndrome. *Experimental eye research* 1991;53:685-690.
9. Hood DC, Cideciyan AV, Román AJ, Jacobson SG. Enhanced S cone syndrome: evidence for an abnormally large number of S cones. *Vision Research* 1995;35:1473-1481.
10. Greenstein VC, Zaidi Q, Hood DC, Spehar B, Cideciyan AV, Jacobson SG. The enhanced S cone syndrome: an analysis of receptor and post-receptor changes. *Vision Research* 1996;36:3711-3722.

11. Audo I, Michaelides M, Robson AG, et al. Phenotypic variation in enhanced S-cone syndrome. *Investigative Ophthalmology and Visual Science* 2008;49:2082-2093.
12. Milam AH, Rose L, Cideciyan AV, et al. The nuclear receptor NR2E3 plays a role in human retinal photoreceptor differentiation and degeneration. *Proceedings of the National Academy of Sciences* 2002;99:473-478.
13. Park SP, Hong IH, Tsang SH, et al. Disruption of the human cone photoreceptor mosaic from a defect in NR2E3 transcription factor function in young adults. *Graefe's archive for clinical and experimental ophthalmology = Albrecht von Graefes Archiv fur klinische und experimentelle Ophthalmologie* 2013;1-11.
14. Kobayashi M, Takezawa S, Hara K, et al. Identification of a photoreceptor cell-specific nuclear receptor. *Proceedings of the National Academy of Science USA* 1999;96:4814-4819.
15. Cheng H, Khanna H, Oh ECT, Hicks D, Mitton KP, Swaroop A. Photoreceptor-specific nuclear receptor NR2E3 functions as a transcriptional activator in rod photoreceptors. *Human Molecular Genetics* 2004;13:1563-1575.
16. Bumsted O'Brien KM, Cheng H, Jiang Y, Schulte D, Swaroop A, Hendrickson AE. Expression of photoreceptor-specific nuclear receptor NR2E3 in rod photoreceptors of fetal human retina. *Investigative Ophthalmology and Visual Science* 2004;45:2807-2812.
17. Peng G-H, Ahmad O, Ahmad F, Liu J, Chen S. The photoreceptor-specific nuclear receptor Nr2e3 interacts with Crx and exerts opposing effects on the transcription of rod versus cone genes. *Human Molecular Genetics* 2005;14:747-764.
18. Chen J, Rattner A, Nathans J. The rod photoreceptor-specific nuclear receptor Nr2e3 represses transcription of multiple cone-specific genes. *Journal of Neuroscience* 2005;25:118-129.
19. Cheng H, Aleman TS, Cideciyan AV, Khanna R, Jacobson SG, Swaroop A. *In vivo* function of the orphan nuclear receptor NR2E3 in establishing photoreceptor identity during mammalian retinal development. *Human Molecular Genetics* 2006;15:2588-2602.
20. Haider NB, Naggert JK, Nishina PM. Excess cone cell proliferation due to lack of a functional NR2E3 causes retinal dysplasia and degeneration in rd7/rd7 mice. *Human Molecular Genetics* 2001;10:1619-1626.
21. Sharon D, Sandberg MA, Caruso RC, Berson EL, Dryja TP. Shared mutations in NR2E3 in enhanced S-cone syndrome, Goldmann-Favre syndrome, and many cases of clumped pigmentary retinal degeneration. *Archives of Ophthalmology* 2003;121:1316-1323.
22. Wright AF, Reddick AC, Schwartz SB, et al. Mutation analysis of NR2E3 and NRL genes in Enhanced S cone syndrome. *Human Mutation* 2004;24:439.

23. Schorderet DF, Escher P. NR2E3 mutations in enhanced S-cone sensitivity syndrome (ESCS), Goldmann-Favre syndrome (GFS), clumped pigmentary retinal degeneration (CPRD), and retinitis pigmentosa (RP). *Human Mutation* 2009;30:1475-1485.
24. Hecht S, Smith EL. Intermittent stimulation by light. VI. Area and the relation between critical frequency and intensity. *Journal of General Physiology* 1936;19:979-989.
25. Tyler CW, Hamer RD. Analysis of visual modulation sensitivity. IV. Validity of the Ferry-Porter law. *Journal of the Optical Society of America A* 1990;7:743-758.
26. Brindley GS, Du Croz JJ, Rushton WAH. The flicker fusion frequency of the blue-sensitive mechanism of colour vision. *Journal of Physiology* 1966;183:497-500.
27. Marks LE, Bornstein MH. Spectral sensitivity by constant CFF: effect of chromatic adaptation. *Journal of the Optical Society of America* 1973;63:220-226.
28. Stockman A, MacLeod DIA, DePriest DD. The temporal properties of the human short-wave photoreceptors and their associated pathways. *Vision Research* 1991;31:189-208.
29. Baylor DA, Nunn BJ, Schnapf JL. Spectral sensitivity of cones of the monkey *Macaca fascicularis*. *Journal of Physiology* 1987;390:145-160.
30. Schnapf JL, Nunn BJ, Meister M, Baylor DA. Visual transduction in cones of the monkey *Macaca fascicularis*. *Journal of Physiology* 1990;427:681-713.
31. Stockman A, Plummer DJ. Color from invisible flicker: a failure of the Talbot-Plateau law caused by an early "hard" saturating nonlinearity used to partition the human short-wave cone pathway. *Vision Research* 1998;38:3703-3728.
32. Mollon JD, Krauskopf J. Reaction time as a measure of the temporal response properties of individual colour mechanisms. *Vision Research* 1973;13:27-40.
33. Smith VC, Bowen RW, Pokorny J. Threshold temporal integration of chromatic stimuli. *Vision Research* 1984;24:653-660.
34. Schrödinger E. Über das Verhältnis der Vierfarben zur Dreifarben Theorie. *Sitzungsberichte Abt 2a, Mathematik, Astronomie, Physik, Meteorologie und Mechanik Akademie der Wissenschaften in Wien, Mathematisch-Naturwissenschaftliche Klasse* 1925;134:471.
35. Luther R. Aus dem Gebiet der Farbmetrik. *Zeitschrift für technische Physik* 1927;8:540-558.
36. Walls GL. A branched-pathway schema for the color-vision system and some of the evidence for it. *American Journal of Ophthalmology* 1955;39:8-23.
37. de Lange H. Research into the dynamic nature of the human fovea-cortex systems with intermittent and modulated light. II. Phase shift in brightness and delay in color perception. *Journal of the Optical Society of America* 1958;48:784-789.

38. Guth SL, Alexander JV, Chumbly JI, Gillman CB, Patterson MM. Factors affecting luminance additivity at threshold among normal and color-blind subjects and elaborations of a trichromatic-opponent color theory. *Vision Research* 1968;8:913-928.
39. Kelly DH. Spatio-temporal frequency characteristics of color-vision mechanisms. *Journal of the Optical Society of America* 1974;64:983-990.
40. Smith VC, Pokorny J. Spectral sensitivity of the foveal cone photopigments between 400 and 500 nm. *Vision Research* 1975;15:161-171.
41. Boynton RM. *Human Color Vision*. New York: Holt, Rinehart and Winston; 1979.
42. Eisner A, MacLeod DIA. Blue sensitive cones do not contribute to luminance. *Journal of the Optical Society of America* 1980;70:121-123.
43. Wisowaty JJ, Boynton RM. Temporal modulation sensitivity of the blue mechanism: measurements made without chromatic adaptation. *Vision Research* 1980;20:895-909.
44. Stockman A, MacLeod DIA, DePriest DD. An inverted S-cone input to the luminance channel: evidence for two processes in S-cone flicker detection. *Invest Ophth Vis Sci* 1987;28:92.
45. Lee J, Stromeyer CF, III. Contribution of human short-wave cones to luminance and motion detection. *Journal of Physiology* 1989;413:563-593.
46. Ripamonti C, Woo WL, Crowther E, Stockman A. The S-cone contribution to luminance depends on the M- and L-cone adaptation levels: silent surrounds? *Journal of Vision* 2009;9:10.11-10.
47. Stockman A, Plummer DJ, Montag ED. Spectrally-opponent inputs to the human luminance pathway: slow +M and -L cone inputs revealed by intense long-wavelength adaptation. *Journal of Physiology* 2005;566:61-76.
48. Stockman A, MacLeod DIA, Lebrun S. Faster than the eye can see: blue cones respond to rapid flicker. *Journal of the Optical Society of America A* 1993;10:1396-1402.
49. Mollon JD, Polden PG. Saturation of a retinal cone mechanism. *Nature* 1977;259:243-246.
50. Stromeyer CF, III, Kronauer RE, Madsen JC. Response saturation of short-wavelength cone pathways controlled by color-opponent mechanisms. *Vision Research* 1979;19:1025-1040.
51. Hecht S, Verrijp CD. The influence of intensity, color and retinal location on the fusion frequency of intermittent illumination. *Proceedings of the National Academy of Sciences of the United States of America* 1933;19:522-535.
52. Hecht S, Schlaer S. Intermittent stimulation by light. V. The relation between intensity and critical frequency for different parts of the spectrum. *Journal of General Physiology* 1936;19:965-977.
53. Hartline HK, Wagner HG, Ratliff F. Inhibition in the eye of *Limulus*. *Journal of General Physiology* 1956;39:651-656.

54. Ratliff F, Hartline HK, Miller WH. Spatial and temporal aspects of retinal inhibitory interaction. *Journal of the Optical Society of America* 1963;53:110-120.
55. Dacey DM, Lee BB, Stafford DK, Pokorny J, Smith VC. Horizontal cells of the primate retina: cone specificity without spectral opponency. *Science* 1996;271:656-659.
56. Calkins DJ. Seeing with S cones. *Progress in Retinal and Eye Research* 2001;20:255-287.
57. Boycott BB, Hopkins JM, Sperling HG. Cone connections of the horizontal cells of the rhesus monkey's retina. *Proceedings of the Royal Society of London Series B* 1987;229:345-379.
58. Goodchild AK, Chan TL, Grünert U. Horizontal cell connections with short-wavelength-sensitive cones in macaque monkey retina. *Visual Neuroscience* 1996;13:833-845.
59. Watson AB. Temporal sensitivity. In: Boff K, Kaufman L, Thomas J (eds), *Handbook of Perception and Human Performance*. New York: Wiley; 1986:6-1-6-43.
60. Mollon JD, Polden PG. An anomaly in the response of the eye to light of short wavelengths. *Philosophical Transactions of the Royal Society of London Series B* 1977;278:207-240.
61. Mollon JD. Color Vision. *Annual Review of Psychology* 1982;33:41-85.
62. Jones BW, Watt CB, Frederick JM, et al. Retinal remodeling triggered by photoreceptor degenerations. *Journal of Comparative Neurology* 2003;464:1-16.
63. Marc RE, Jones BW, Watt CB, Strettoi E. Neural remodeling in retinal degeneration. *Progress in Retinal and Eye Research* 2003;22:607-655.
64. Humanski RA, Wilson HR. Spatial frequency mechanisms with short-wavelength-sensitive cone inputs. *Vision Research* 1992;32:549-560.
65. van Nes FL, Bouman MA. Spatial modulation transfer in the human eye. *Journal of the Optical Society of America* 1967;57:401-406.
66. Granit R, Harper P. Comparative studies on the peripheral and central retina. II. Synaptic reactions in the eye. *American Journal of Physiology* 1930;95:211-228.
67. Kugelmass S, Landis C. The Relation of Area and Luminance to the Threshold for Critical Flicker Fusion. *American Journal of Psychology* 1955;68:1-19.
68. Simonson E, Brožek J. Flicker fusion frequency: background and applications. *Physiological Reviews* 1952;32:349-378.
69. Landis C. Determinants of the critical flicker-fusion threshold. *Physiological Reviews* 1954;34:259-286.
70. de Lange H. Research into the dynamic nature of the human fovea-cortex systems with intermittent and modulated light. I. Attenuation characteristics with white and colored light. *Journal of the Optical Society of America* 1958;48:777-784.

71. Kelly DH. Flicker fusion and harmonic analysis. *Journal of the Optical Society of America* 1961;51:917-918.
72. Hamer RD, Tyler CW. Analysis of visual modulation sensitivity. V. Faster visual response for G- than for R-cone pathway? *Journal of the Optical Society of America A* 1992;9:1889-1904.
73. Tyler CW. Analysis of visual modulation sensitivity. II. Peripheral retina and the role of photoreceptor dimensions. *Journal of the Optical Society of America A* 1985;2:393-398.
74. Tyler CW, Hamer RD. Eccentricity and the Ferry-Porter law. *Journal of the Optical Society of America A* 1993;10:2084-2087.
75. Rovamo J, Raninen A. Critical flicker frequency as a function of stimulus area and luminance at various eccentricities in human cone vision: A revision of Granit-Harper and Ferry-Porter laws. *Vision Research* 1988;28:785-790.
76. Curcio CA, Allen KA. Topography of ganglion cells in human retina. *Journal of Comparative Neurology* 1990;300:5-25.
77. Tyler CW. Analysis of human receptor density. In: Lakshminarayanan V (ed), *Basic and Clinical Applications of Vision Science: the Professor Jay M Enoch Festschrift Volume*. Berlin: Springer; 1977:63-71.
78. Østerberg GA. Topography of the layer of rods and cones in the human retina. *Acta Ophthalmologica (supplement)* 1935;6:1-102.
79. Elsner AE, Burns SA, Webb RH. Mapping cone photopigment optical density. *Journal of the Optical Society of America A* 1993;10:52-58.
80. Ferry J. Persistence of vision. *American Journal of Science and Arts* 1892;44:192-207.
81. Porter TC. Contributions to the study of flicker. II. *Proceedings of the Royal Society of London Series A* 1902;70:313-319.
82. Stockman A, Langendörfer M, Smithson HE, Sharpe LT. Human cone light adaptation: from behavioral measurements to molecular mechanisms. *Journal of Vision* 2006;6:1194-1213.
83. Stockman A, Smithson HE, Michaelides M, Moore AT, Webster AR, Sharpe LT. Residual cone vision without α -transducin. *Journal of Vision* 2007;7:8.1-13.
84. Stockman A, Smithson HE, Webster AR, et al. The loss of the PDE6 deactivating enzyme, RGS9, results in precocious light adaptation at low light levels. *Journal of Vision* 2008;8:10.11-10.

FIGURE LEGENDS

Figure 1. S-cone critical flicker fusion frequencies (Hz) measured on a 620-nm background of 11.41 \log_{10} quanta $s^{-1} \text{ deg}^{-2}$ plotted as a function of the \log_{10} mean radiance of the 440-nm flickering target.

Data are plotted for each of the six ESCS observers in separate panels: ES1 (yellow circles), ES2 (red circles), ES3 (green circles), ES4 (orange circles), ES5 (violet circles) and ES6 (light blue circles). Each panel also shows the mean data for 12 normal observers (dark blue squares). The small open circles in each panel show the ESCS data below $9.0 \log \text{ quanta s}^{-1} \text{ deg}^{-2}$ shifted vertically to align with the normal data using a least-squares fitting criterion. In all figures, the error bars are ± 1 standard error of the mean (s.e.m.) within observers for the ESCS measurements, and between observers for the normal measurements. ES5 made only one set of measurements.

Figure 2. L-cone critical flicker fusion frequencies measured on a 481-nm background of $8.26 \log_{10} \text{ quanta s}^{-1} \text{ deg}^{-2}$ plotted as a function of the \log_{10} mean radiance of a 650-nm flickering target. Data are plotted for four ESCS observers in separate panels: ES1 (yellow circles), ES2 (red circles), ES3 (green circles) and ES4 (orange circles). Each panel also shows the mean data for 12 normal observers (dark red squares). The error bars are ± 1 standard error of the mean (s.e.m.) within observers for the ESCS measurements, and between observers for the normal measurements.

Figure 3. \log_{10} S-cone modulation sensitivities measured using a sinusoidally flickering 440-nm target superimposed on a steady 620-nm background of $11.41 \log_{10} \text{ quanta s}^{-1} \text{ deg}^{-2}$ plotted as a function of temporal frequency (logarithmic axis). The top, middle and bottom rows of panels show data for high, medium and low 440-nm target radiances of 9.61, 8.73 and $7.40 \log_{10} \text{ quanta s}^{-1} \text{ deg}^{-2}$, respectively. The left-hand, middle and right-hand columns show data for ES1 (yellow symbols), ES2 (red symbols) and ES3 (green symbols), respectively. The data for the ESCS observers are plotted as circles (high level), triangles (medium level) and inverted triangles (low level). In each panel, the mean normal data are plotted as dark-blue squares. The error bars are ± 1 standard error of the mean (s.e.m.) within observers for the ESCS measurements, and between observers for the normal measurements. The red continuous lines show fits of a two-signal S-cone model described in the text.

Figure 4. S-cone versus L/M-cone phase delays (degrees, linear scale) measured between a flickering 440-nm target with a mean radiance of $8.73 \log_{10} \text{ quanta s}^{-1} \text{ deg}^{-2}$ and a flickering 610-nm target with a mean radiance of either 10.32 (ES1), 9.95 (ES2), or 10.04 (ES3) $\log_{10} \text{ quanta s}^{-1} \text{ deg}^{-2}$. The phase delays (degrees) are plotted linearly as a function of temporal frequency (Hz, logarithmic axis) for ES1 (yellow circles), ES2 (red circles) and ES3 (green circles). The two flickering targets were superimposed on a 620-nm background of $11.41 \log_{10} \text{ quanta s}^{-1} \text{ deg}^{-2}$. In each panel, the mean

normal S-cone phase delays are plotted as dark-blue diamonds. The continuous lines are versions of a model in which it is assumed that the S-cone phase delay can be accounted for by the interaction between a delayed, negative S-cone signal and fast, positive one (see Equations [3] and [6]). The green horizontal lines show the predictions if there were only a fast signal (with the same delay as the L/M-cone signal). The blue line shows best-fitting versions of the model applied to the normal data in which the fast signal is set zero (the best-fitting delay relative to L/M-cone flicker is 39.6 ms). The red lines are best-fitting versions of the model fitted to each ESCS data set (see Table 2 for the best-fitting parameters). Lastly, the fine black lines are phase delay predictions based on the model fitted to the temporal contrast functions also measured at the medium level (see middle row of Figure 3 and Table 1)

Figure 5. Vector addition: the weighted “center” signal A_c (white arrow) and “surround” signal A_s (grey arrow), are added with a phase shift of $\Delta\theta$ (red arc) to produce the resultant vector A_r (black arrow) with phase shift of ϕ relative to the centre signal (green arc). The components of the “surround” signal that are in phase and 90° out-of-phase with the “center” signal are also indicated.

Figure A. Upper panel: The mean critical flicker fusion frequencies (Hz) for two observers (ES and SK) for luminance levels of 1.24 (blue diamonds), 1.64 (cyan inverted triangles), 2.44 (green squares), 3.04 (yellow triangles) and 3.64 (red circles) log phot. td. replotted from Table 1 of Kugelmass & Landis⁶⁷ as a function of the logarithm of target area (log deg²) and vertically shifted to align with their mean between 2.98 and 7.10° deg of visual angle in diameter; i.e. aligned between the vertical red line labelled 2.98 and that labelled 7.10 and containing our 4° target diameter. Over this range, the data can be well approximated by a linear function, as shown by the black line, the equation for which is given by Equation [A1]. The dashed lines show the Equation [A1] extended outside the fitted range. The troland values were converted from mL (milli-Lamberts) by assuming a 2-mm pupil diameter. See text for other details.

Bottom panel: The mean critical flicker fusion data from Kugelmass & Landis⁶⁷ from 2.98° to 7.10° deg of visual angle in diameter from the upper panel replotted as a function of the logarithm of cone number. Symbols as in the upper panel. The shifted data can be approximated by the linear function (black line) given by Equation [A4].

Figure B. Cone density (cones per deg²) plotted as a function of retinal eccentricity (degrees) for human temporal retina (yellow circles) taken from Figure 6 of Curcio et al⁷⁶ (their open squares). A continuous exponential function (red line, given by Equation [A2]) was fitted to the densities from 0° to 60° of eccentricity.

TABLE LEGENDS

Table 1. The best-fitting parameters and their standard errors and R^2 values for the model given by Equations [3] and [4] fitted to the S-cone modulation sensitivity data for ES1, ES2 and ES3 at the High, Medium and Low adaptation levels. See text for details.

Table 2. The best-fitting parameters and their standard errors and R^2 values of the model given by Equations [3] and [6] fitted to the S-cone phase delay data for ES1, ES2 and ES3 measured at the Medium adaptation level. See text for details.

FIGURE 1

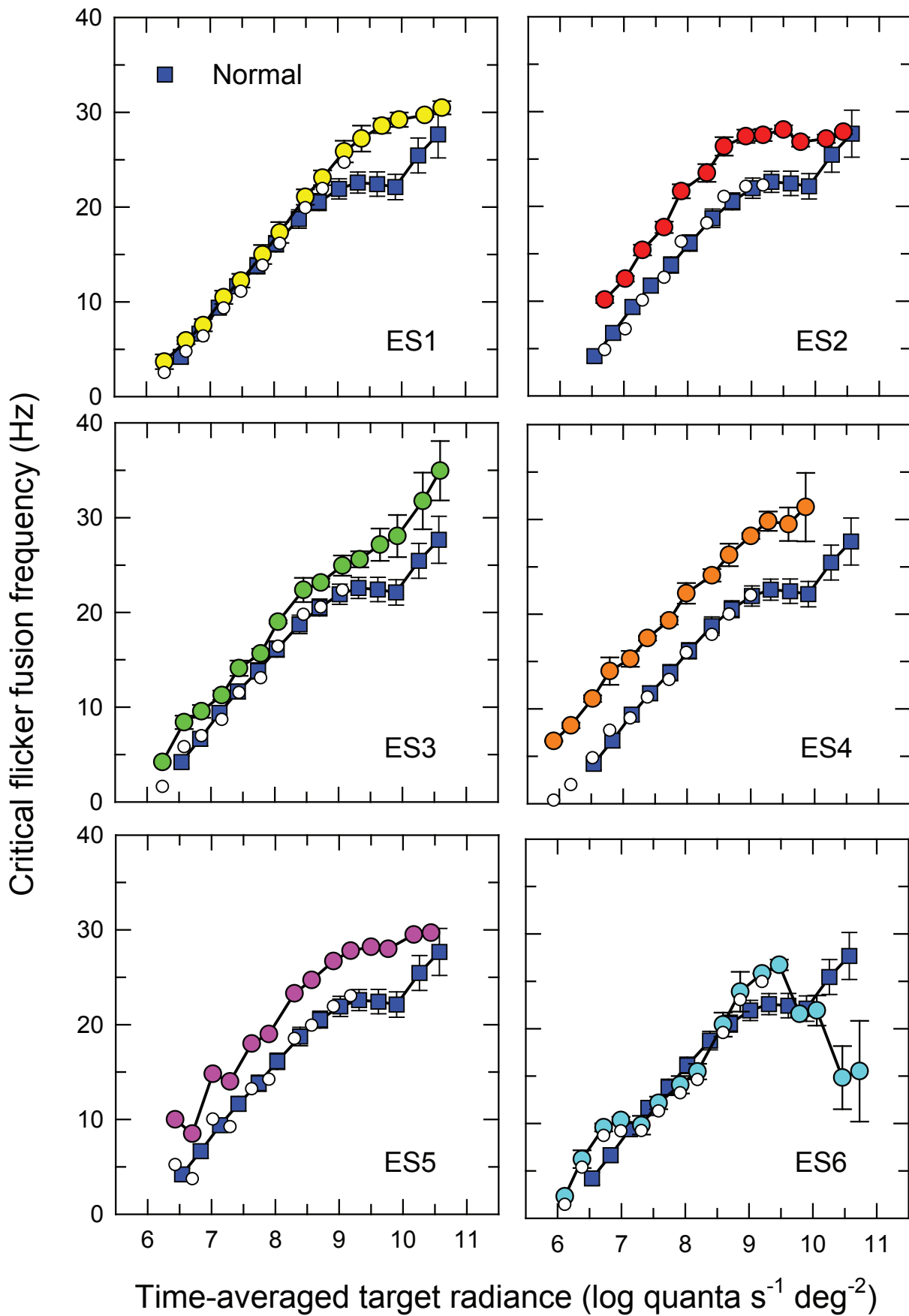


FIGURE 2

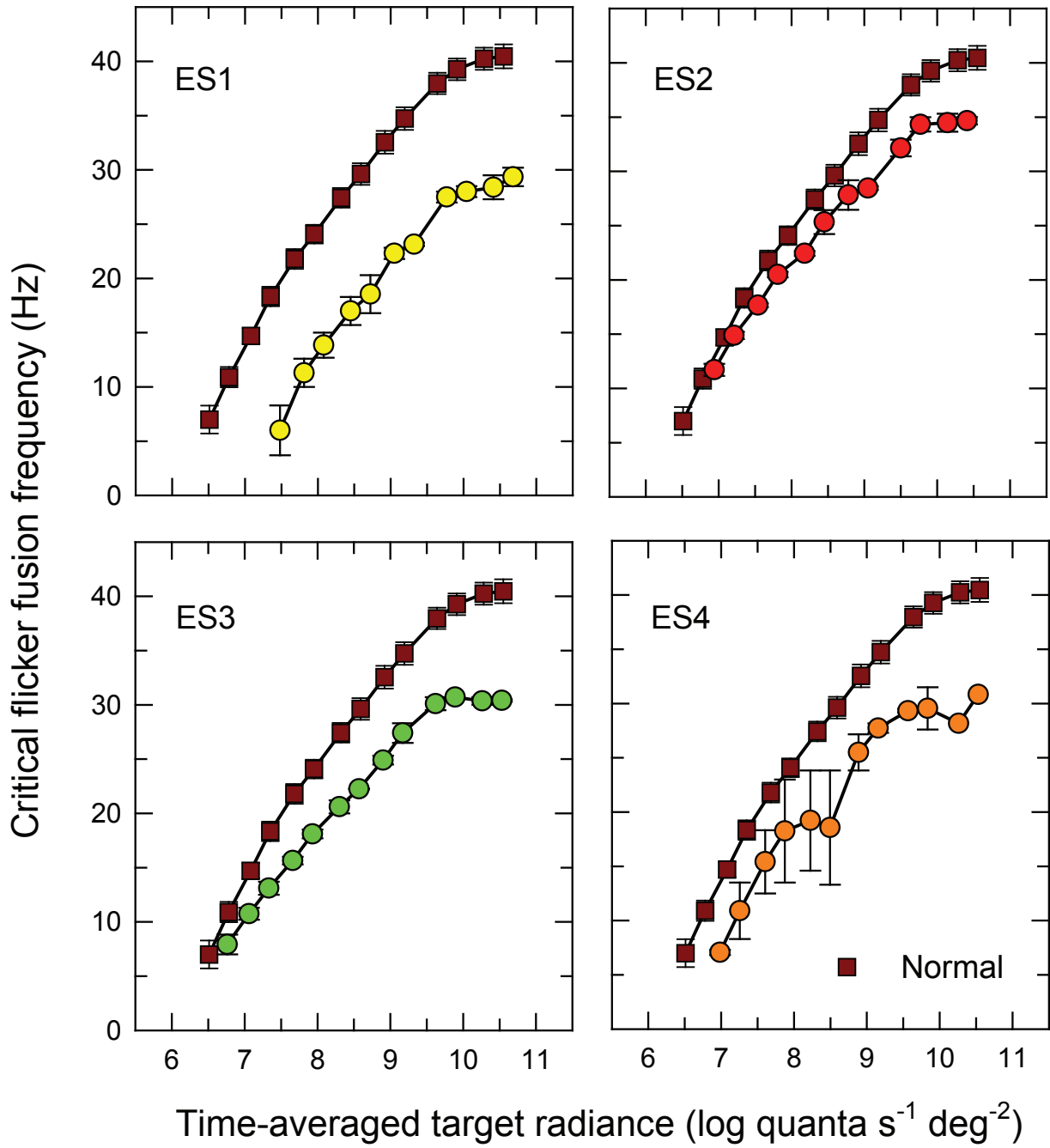


FIGURE 3

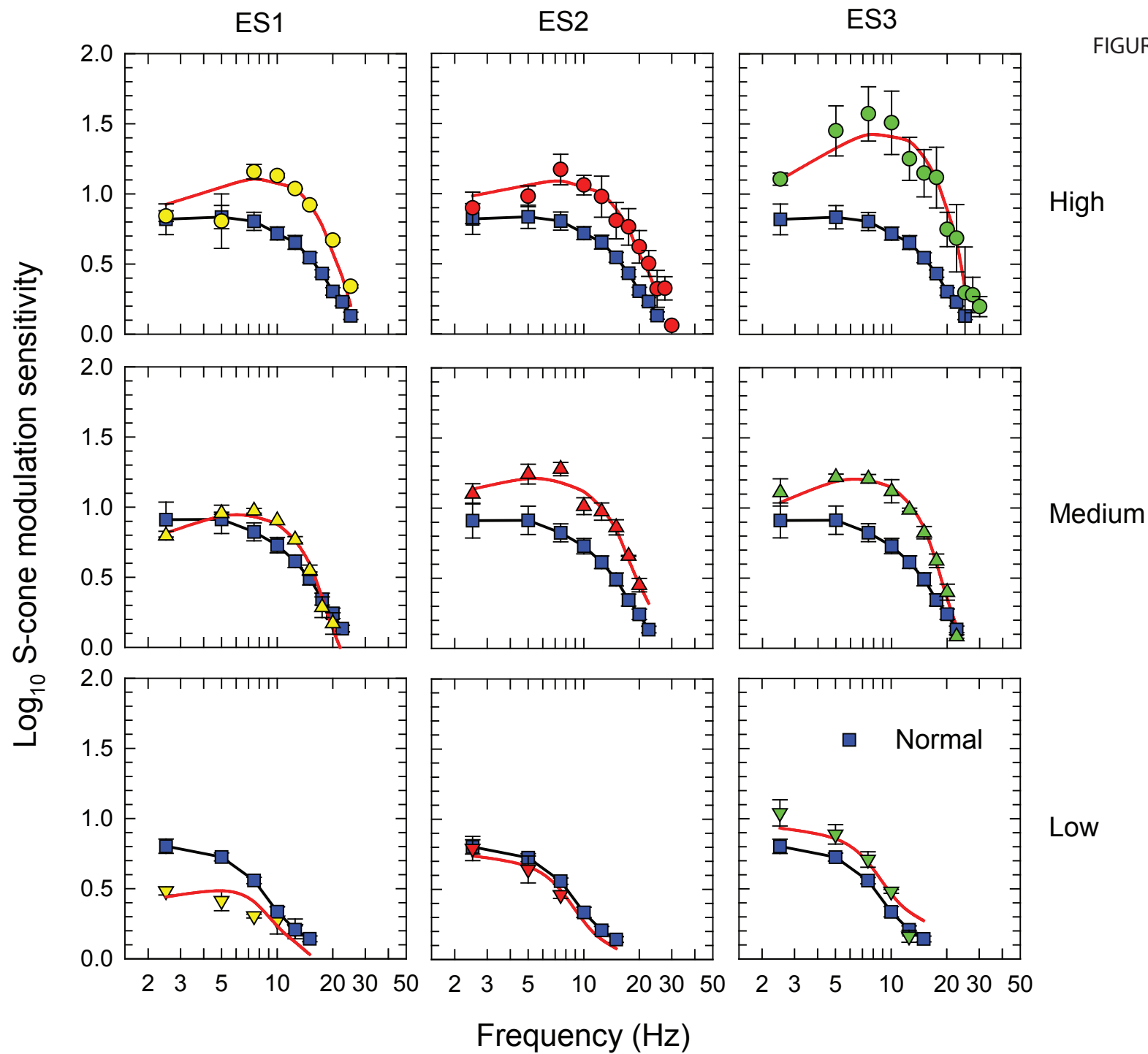


FIGURE 4

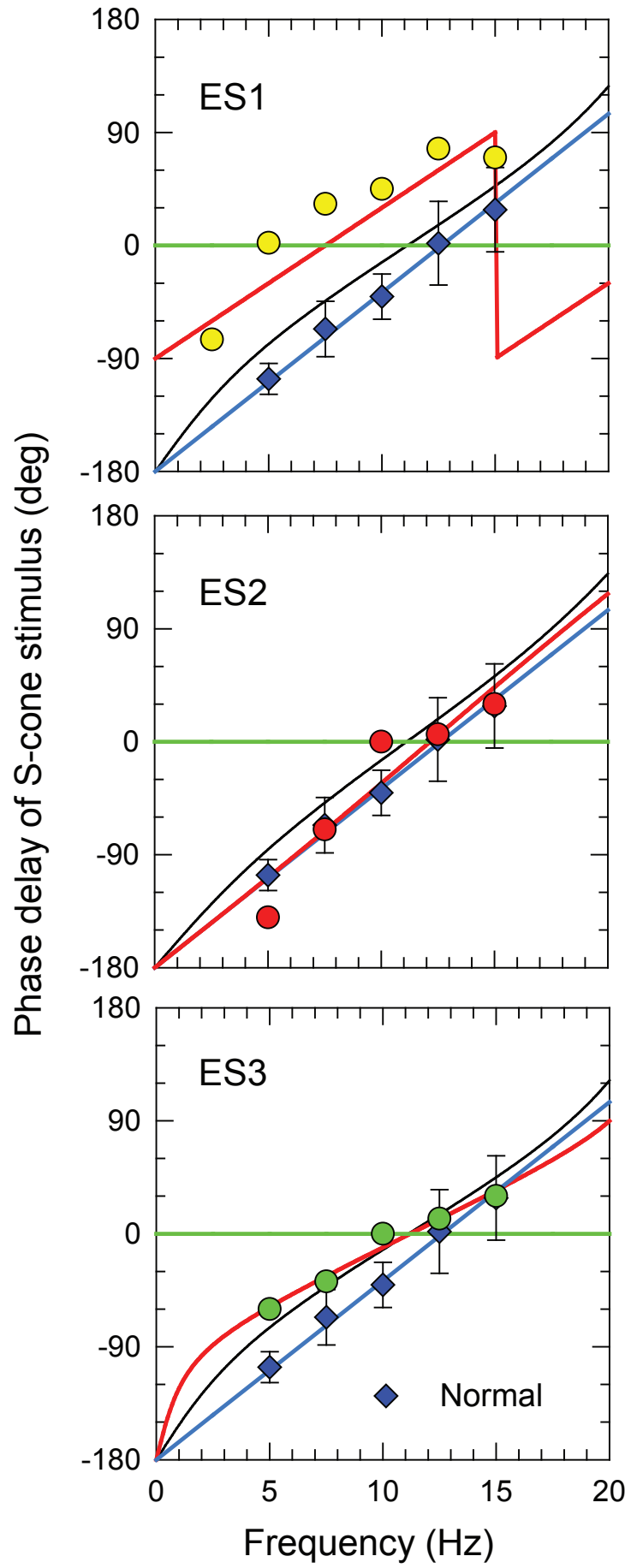


FIGURE 5

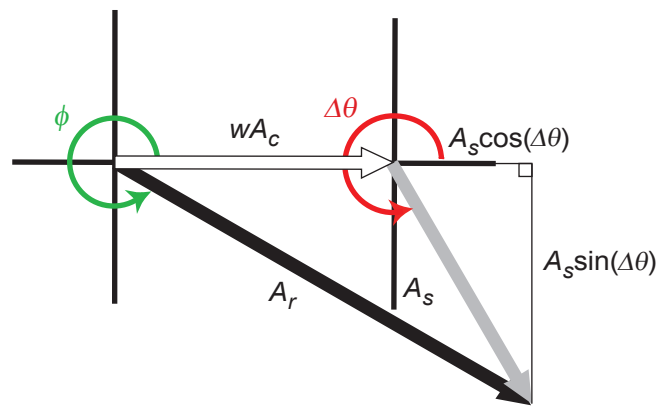


FIGURE A

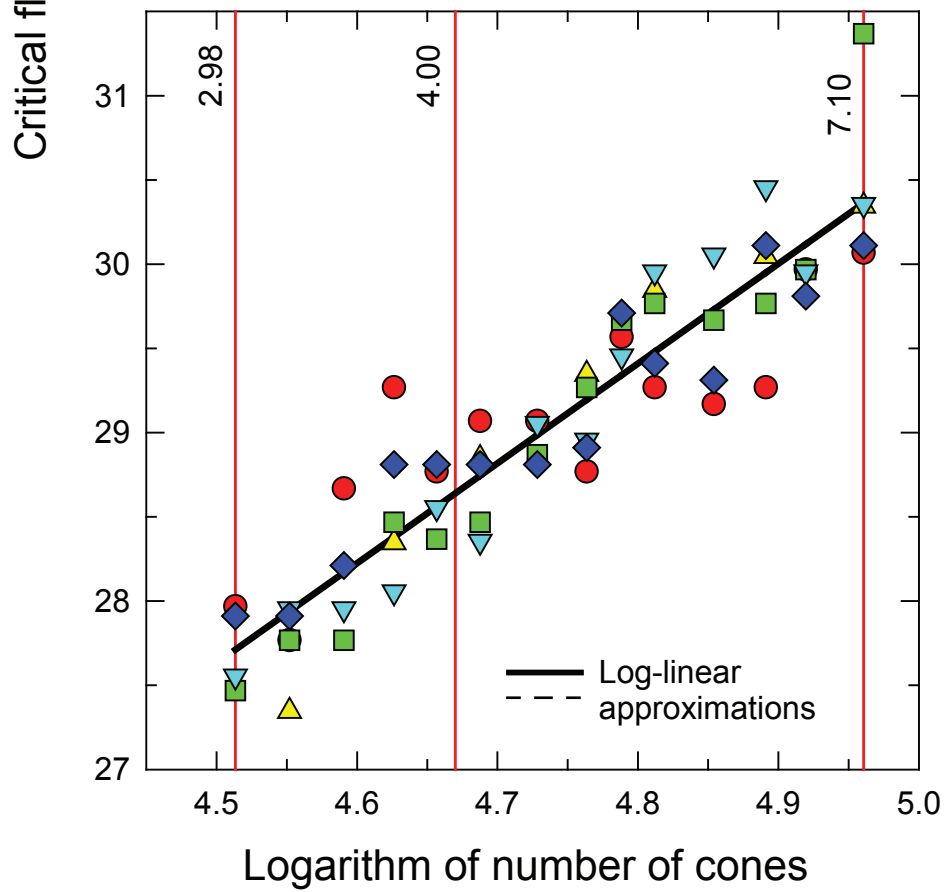
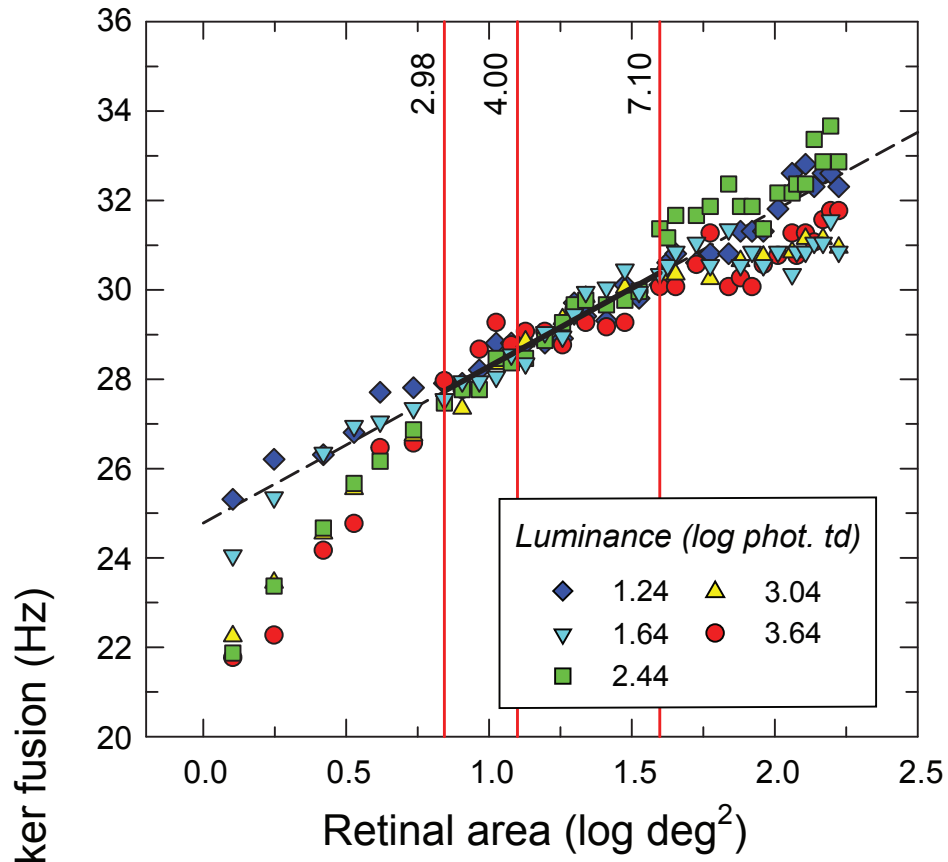


FIGURE B

